CDF/PUB/ELECTROWEAK/PUBLIC/10648

Search for the Associated Production of Higgs and W Bosons in the $WH \to \tau\nu b\bar{b}$ final state, with 5.7 fb^{-1} of CDF Data

The CDF Collaboration
URL http://www-cdf.fnal.gov
(Dated: September 2, 2011)

We present a search for the associated production of the standard model Higgs boson and a W boson. The search is performed using data corresponding to an integrated luminosity of 5.7fb^{-1}, collected by the CDF detector at the Tevatron in $p\bar{p}$ collisions at $\sqrt{s} = 1.96$ TeV. $WH \to \tau\nu b\bar{b}$ candidate events are selected requiring two jets, a hadronically decaying τ lepton and large missing transverse energy. In addition, at least one of the jets must be consistent with originating from a bottom quark. A binned likelihood fit of the di-jet invariant mass distribution is performed to test for a potential Higgs boson signal. With no signal observed, we set upper limits on the Higgs boson cross section time branching ratio B($H \to b\bar{b}$) as a function of its mass. For the Higgs boson mass of 115 GeV/c^2 the observed (expected) upper limits is 28.7 (46.6) $\times$ the Standard Model expectation.

Preliminary Results

I. INTRODUCTION

If the Higgs boson is light, as the indirect and direct constrains suggest [1] [3] [2], it decays mostly to $b\bar{b}$ pairs, with a branching fraction that varies between 80.3 % for $m_H = 100$ GeV/c^2 down to 16.7 % for $m_H = 150$ GeV/c^2. The main Higgs boson production mechanism at the Tevatron is gluon fusion, that produces one Higgs boson and nothing else. The signal is then characterized by a bottom-anti bottom pair, that is not distinguishable from the SM bottom-quark pair production. The associated production of the Higgs boson with a W is the second highest production cross section at the Tevatron, and the presence of an extra lepton from the W decay is helpful in reducing the background. Data analysis that target this final state set some of the most stringent limits at the Tevatron. The most recent CDF searche for WH associated production[4] studies events where an electron or muon is reconstructed. To increase the acceptance to the signal, it also considers events where an isolated track is present, including some $W \to \tau\nu$ events. However it does not target events containing τs, that instead are the main focus of this work.

This note details a search for a low mass Higgs boson, when produced in association with a W boson, in the $WH \to \tau\nu b\bar{b}$ final state. Tau lepton has a mean lifetime of 0.290 ps, and can be detected only through its decay products. It decays into electrons or muons 35% of the time, while the rest of the time it decays into charged and neutral pions or other hadrons. Electrons and muons produced in τ decays are indistinguishable from the prompt ones, and are included in the existing analysis, so the final state considered in this work is characterized by a hadronically decaying τs, missing transverse energy and two energetic jets.

II. DETECTOR AND DATA SAMPLE

The CDF II detector is a magnetic spectrometer with cylindrical symmetry around the beam pipe, surrounded by calorimeters and muon detectors. It is described in details in [5] and [6]. The geometry is described using the azimuthal angle Φ and pseudorapidity $\eta = -ln\tan\theta/2$, where θ is the polar angle with respect to the proton beam axis. The charge particle tracking system consists, in its innermost component, of six layers of double-sided silicon-microstrip sensors at radii between 2.5 and 22 cm from the beam, covering a region $|\eta| < 2$. It reconstructs displaced tracks with a resolution of 15 μm, and it is an essential component of the B-hadron identification. It is surrounded by a 96-layer drift chamber, with coverage $|\eta| < 1$, immersed in a 1.4 T solenoidal magnetic field, parallel to the particle beam. Outside the solenoid there are sampling electromagnetic and hadronic calorimeters.A set of wire and strip chambers, embedded in the calorimeter at a depth of approximatly 6 radiation lenghts, whrere energy deposition of EM showers reaches its maximum, help to distinguish photons from electrons. A Cherenkov luminosity counters is used to measure the the luminosity of $p\bar{p}$ collision at CDF.
We conduct the analysis using data collected by the CDFII detector from February 2002 to February 2010 and corresponding to the integrated luminosity of 5.7 fb^{-1}. The sample used in this analysis is a subset of data acquired by the CDF online selection system (trigger), which requires to events with one narrow, isolated jet with E_T >20 GeV (the τ candidate) and missing transverse energy greater than 20 GeV. Because of the high rate of events accepted by this trigger, it was modified multiple times during the data taking period to cope with the increasing luminosity.

III. EVENT SELECTION

The strategy of this analysis is to loosen the event selection requirements to keep the acceptance to Higgs particles as high as possible, and use the mass of the di-jet system to distinguish the signal from the background.
The hadronically decaying τ is reconstructed in the detector as narrow cluster in the calorimeter, matching reconstructed high p_T tracks (mostly charged pions) and π^0's. The reconstruction algorithm considers the highest p_T track, and builds around it a signal cone with aperture $\theta = 10\,^\circ$. Then, it matches the track with a calorimeter cluster using η and ϕ information.The Shower Max Detector [6] is used to reconstruct the presence of π^0, that, if they fall into the signal cone, are associated with the τ candidate. Since the neutrino is not detected, only a partial reconstruction of the τ momentum is possible: the charged and neutral pions four-momenta are added to build the so called visible four-momentum. The requirements and thresholds used to identify the τ candidate are mostly the offline version of those applied by the trigger. It is possible to suppress the background represented by jets originating from quarks and gluons requiring the τ candidate to be isolated. Both a track based and calorimeter based isolation are used. The former is imposed by demanding no tracks with $p_T > 1$ GeV in the region $10\,^\circ < \theta < 30\,^\circ$ outside the signal cone: the latter, requiring the fraction of energy deposited around the τ cluster to be smaller than 0.10 % of the τ cluster energy. The mass of the decays products is another powerful variable to distinguish real τs and jets: we require it to be smaller than the τ lepton one. Most of electrons which could mimic the hadronic signature are

removed vetoing events that contain an identified electrons. The fraction that survives is removed using the relation $E_m \leq E_{\rm Tot} - 0.15 \times \sum P$, where E_m is the electromagnetic energy deposition, $E_{\rm Tot}$ the total calorimeter energy $\sum P$ the scalar sum of the momentum of all the tracks associated with the tau candidate.
Events in the final sample must contain exactly one hadronically decaying τ reconstructed in the central region ($|\eta|$ ¡ 1., with offline transverse energy of the visible decay products (E_T^{Vis}) > 20 GeV. A good quality reconstructed primary vertex is required to be in the region consistent with the beam-beam interaction. Events that contain an extra muons or isolated track are rejected, to suppress the Drell-Yan background.
Jets are reconstructed energy depositions in the calorimeter towers using a cone clustering algorithm, with cone size $R = \sqrt{(\Delta\Phi)^2 + (\Delta\eta)^2} = 0.4$. They are required to be separated from the identified τ candidate ($\Delta R > 0.4$), have a E_T, corrected for instrumental effects [7], greater than 20 GeV, and $|\eta| < 2$.
The missing transverse energy $\not\!\!E_T$, calculated as the vector sum of all the calorimeter tower energy depositions projected in the transverse plane, is used to determine the presence of neutrinos in the event. Both its magnitude and direction are recalculated after correcting the energy of the jets. The events are classified according to the number of jets. Events that have exactly two jets are selected, while events with a different number of jets are used to validate the event selection and identification procedures.

A. Bottom Quark Tagging Algorithms

Because the Higgs boson decays to $b\bar{b}$ pairs, we can exploit the relatively long lifetime and large mass of the B hadrons to identified jets originating from a bottom quark, and reduce considerably the backgrounds. We require that at least one jet in the event be identified as originating from a b quark by the secondary vertex tagging algorithm (denoted as SecVtx). The SecVtx algorithm reconstructs a secondary vertex inside a jet using tracks with large impact parameter. The secondary vertex is considered displaced from the primary one if its significance is greater than 3. The average displacement resolution is of the order of 190 μm. This method has been used in other Higgs boson searches and in studies of top-quark properties [8]. We use two mutually exclusive tagging categories: events that contain exactly one SecVtx tag (Single Tag), and events that contains two SecVtx tags (Double Tag).

B. Total WH Acceptance

The signal acceptance is estimated in Monte Carlo samples, generated with PYTHIA [9], for Higgs boson mass between 100 and 150 GeV/c^2, in 5 GeV/c^2 steps. The detection efficiency for the signal is defined as:

$$\epsilon_{WH\to\tau\nu b\bar{b}} = \epsilon_{Z0} \cdot SF^{\epsilon_{Z0}} \cdot \epsilon_{trigger} \cdot SF^{\epsilon_{trigger}} \cdot \epsilon_{ID} \cdot SF^{\epsilon_{ID}} \cdot \epsilon_{WH}^{MC} \cdot SF^{\epsilon_{b-tag}} \cdot BR(W \to \tau\nu) \quad (1)$$

where ϵ_{WH}^{MC} is the fraction of the signal events (with $|z0| < 60\ cm$) which satisfy the kinematics and b-tagging requirements. This number is corrected by the b-tag scale factor, $SF^{\epsilon_{b-tag}}$. The efficiency on the z0 cut is determined by the product of the efficiency of the cut in Monte Carlo ϵ_{Z0} and the correction factor accounting for the difference between the data and Monte Carlo efficiency, $SF^{\epsilon_{Z0}}$. The trigger and the identification efficiency are both measured in Monte Carlo. To correct for differences between the efficiency in data and simulation, it is multiplied it by the $SF = SF^{\epsilon_{trigger}} \cdot SF^{\epsilon_{ID}} = 0.72 \pm 0.12$, measured in the sample with 2 jets, before applying the b-tagging condition (Pretag Sample).

IV. BACKGROUNDS

This analysis builds on the method of background estimation detailed in Ref. [8],that was initially developed to predict the composition of a $l + \not\!\!E_T$+jets ($l = e, \mu$) samples, dominated by W+jets. We adapted this method to the sample containing τs, that present a different sample composition.
The dominant background for the current search comes from the multijet production, where the W signature is mimicked by a jet originated from a quark or a gluon, and identified as a τ candidate and by the missing transverse energy arising from the jets energy mis-measurement.We choose to model this background from data, using a multijet-enriched data sample,very similar to the signal sample one, but orthogonal to it. The events are acquired with the same trigger as the signal sample and satisfy the requirements described in section III. To make the multijet-enriched sample orthogonal to the signal one, we require a tau candidate reconstructed in the event to have two tracks in the tau signal cone. Events in the signal sample are required to have tau candidates with one or three

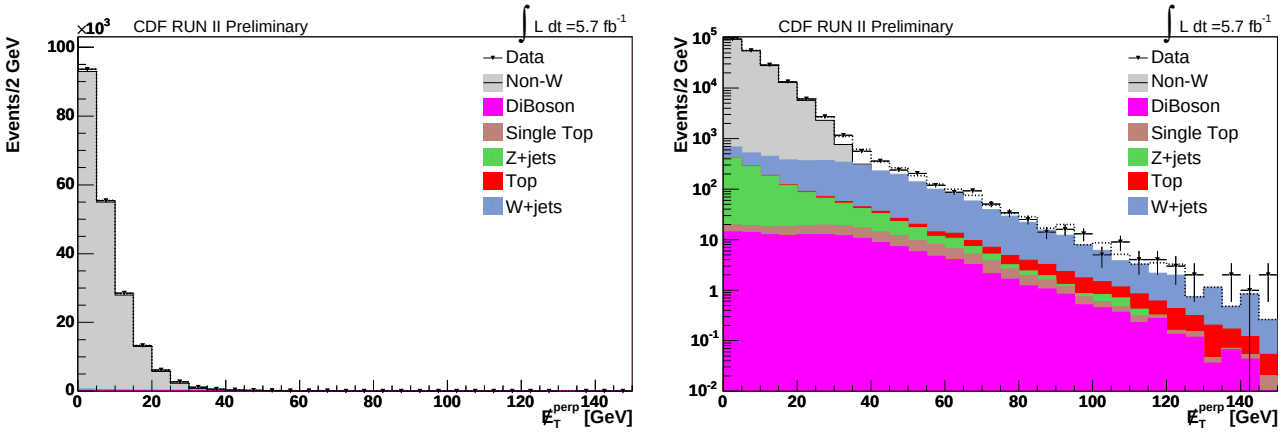

FIG. 1: Likelihood fit of the $\not\!\!E_{\rm T}^{perp}$ distribution in the sample before applying b-tagging (Pretag). The Non-W templates is not added to the sum of the other backgrounds.The dashed histogram represents the sum of all the backgrounds, including Non-W.

tracks. The contribution of real τs in the multijet sample is negligible.

The contributions from the following individual background sources are calculated: W plus light falvor jets that are falsely b-tagged, W production with heavy flavor quark pairs, multijet events with false W signatures, top quark production, and diboson production.

- W + heavy flavor: W + heavy flavor contribution is calculated using information from both data and Monte Carlo samples. We calculate the fraction of W events with associated heavy flavor production in the Monte Carlo samples generated with ALPGEN interfaced with PYTHIA parton shower code [9, 10]. To predict the number of events with a b-tagged jet, this fraction and the b-tagging efficiency are multiplied by the number of W+jets events in the sample prior to applying b-tagging (called pretag sample).

- W+ light flavor jets that are falsely b-tagged (mistag): the number of W+ light flavor events in the pretag sample is the difference between the overall rate of W+jets events and the contribution from the W+ heavy flavor. To estimate the amount of W + light flavor in the tagged sample, we apply a per-jet false tag rate parametrization (mistag matrix) to the pretag W + light flavor events. The mistag matrix is obtained from inclusive jet data.

- Multijet background (non-W): we use the difference in $\not\!\!E_{\rm T}^{perp}$ shape between the multijet and the other background models to constrain the non-W contribution. We perform a likelihood fit to the $\not\!\!E_{\rm T}^{perp}$ distribution to determine the total amount of non-W background present in the pretag and in the b-tagged samples. The missing transverse energy perpendicular, $\not\!\!E_{\rm T}^{perp}$, is the $\not\!\!E_T$ component perpendicular to the closest reconstructed object in the events, either a jet or the τ candidate. It proved to be less correlated with the τ track multiplicity then other variables, for example the $\not\!\!E_T$, so the background model (dominated by the multijet events) better describes the data. Figures 1,2 and 3 show the result of the $\not\!\!E_{\rm T}^{perp}$ fit in the Pretag, Single and Double Tag samples correspondingly.

- Other backgrounds: the expected number of top quark or diboson events is estimated multiplying the acceptance, measured in Monte Carlo and corrected for selection efficiency between data and Monte Carlo, by the process production cross section and the integrated luminosity.

V. SENSITIVITY OPTIMIZATION

The signal samples defined in sections III and III A are dominated by the multijet background, that represent more than 98% of the samples, with a negligible contribution from the signal. The sensitivity of the search in the single and double b-tagged signal samples is optimized separately by varying the $\not\!\!E_{\rm T}^{perp}$ cut. The sensitivity of the search in the single and double b-tagged signal samples is optimized separately by varying the $\not\!\!E_{\rm T}^{perp}$ cut for each background component, and correct the expected number of background events accordingly. We then calculated the 95% confidence level median expected limit on the Higgs production cross section times the $H \to b\bar{b}$ branching ratio

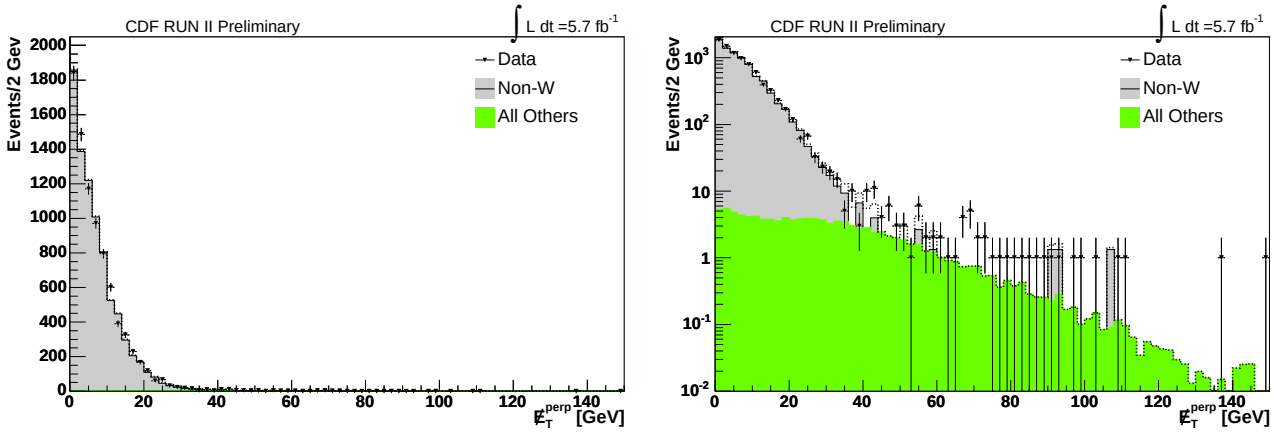

FIG. 2: Likelihood fit of the $\not\!\!E_{\rm T}^{perp}$ distribution in the sample with one b-tagged jet (Single Tag). The Non-W templates is not added to the sum of the other backgrounds.The dashed histogram represents the sum of all the backgrounds, including Non-W.

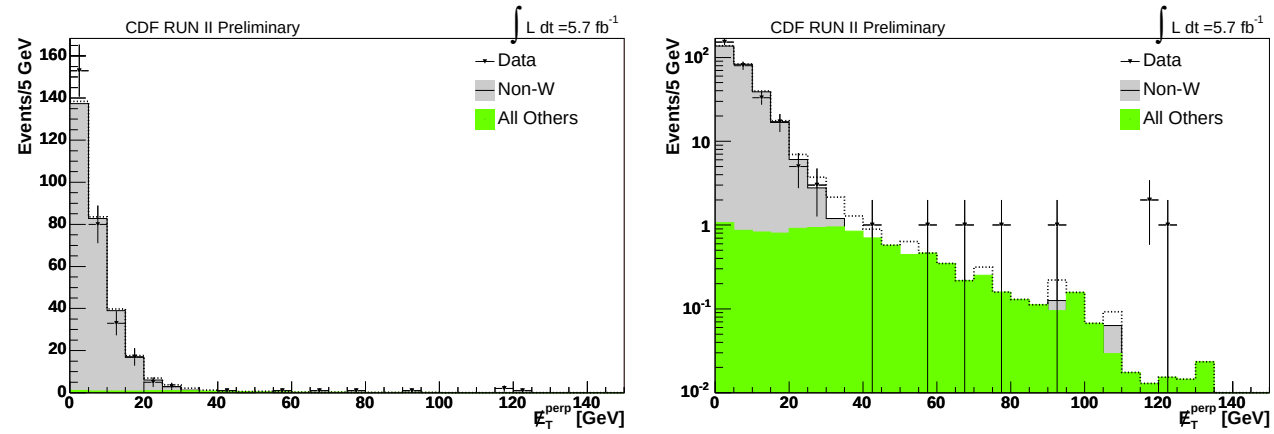

FIG. 3: Likelihood fit of the $\not\!\!E_{\rm T}^{perp}$ distribution in the sample with two b-tagged jets (Double Tag). The Non-W templates is not added to the sum of the other backgrounds.The dashed histogram represents the sum of all the backgrounds, including Non-W.

for the test Higgs boson mass of $m_H = 115 GeV/c^2$, as a function of the $\not\!\!E_{\rm T}^{perp}$ threshold. The bayesian limit is calculated performing a binned likelihood fit of the di-jet mass. The background and signal rates are allowed to vary in the fit, within their systematic uncertainty. Optimization results in the following $\not\!\!E_{\rm T}^{perp}$ cut values:

- $\not\!\!E_{\rm T}^{perp} > 34$ GeV for the ST sample
- $\not\!\!E_{\rm T}^{perp} > 20$ GeV for the ST-ST sample

Table I and II shows the backgrounds prediction for the the single and double b-tagged samples after the $\not\!\!E_{\rm T}^{perp}$ cuts are applied. Figures 4 and 5 shows the agreement between data and background predictions for the same samples.

VI. SYSTEMATIC UNCERTAINTIES

The uncertainty on the trigger and τ identification scale factor is the dominant one, together with the multijet background normalization uncertainty. The former one is measured in the pretag sample, and is mostly affected by the uncertainty on the W+jets normalization. The latter one is dominated by the statistical uncertainty on the efficiency of the $\not\!\!E_{\rm T}^{perp}$ requirements, since the multijet enriched sample contains few events, and the efficiency is small. The uncertainty on the heavy flavor fractions only affects the $W+$ heavy flavor background It covers the variations of the MC/data ratio of the heavy flavor fraction in events with different number of jets. Uncertainty on the b-tagging

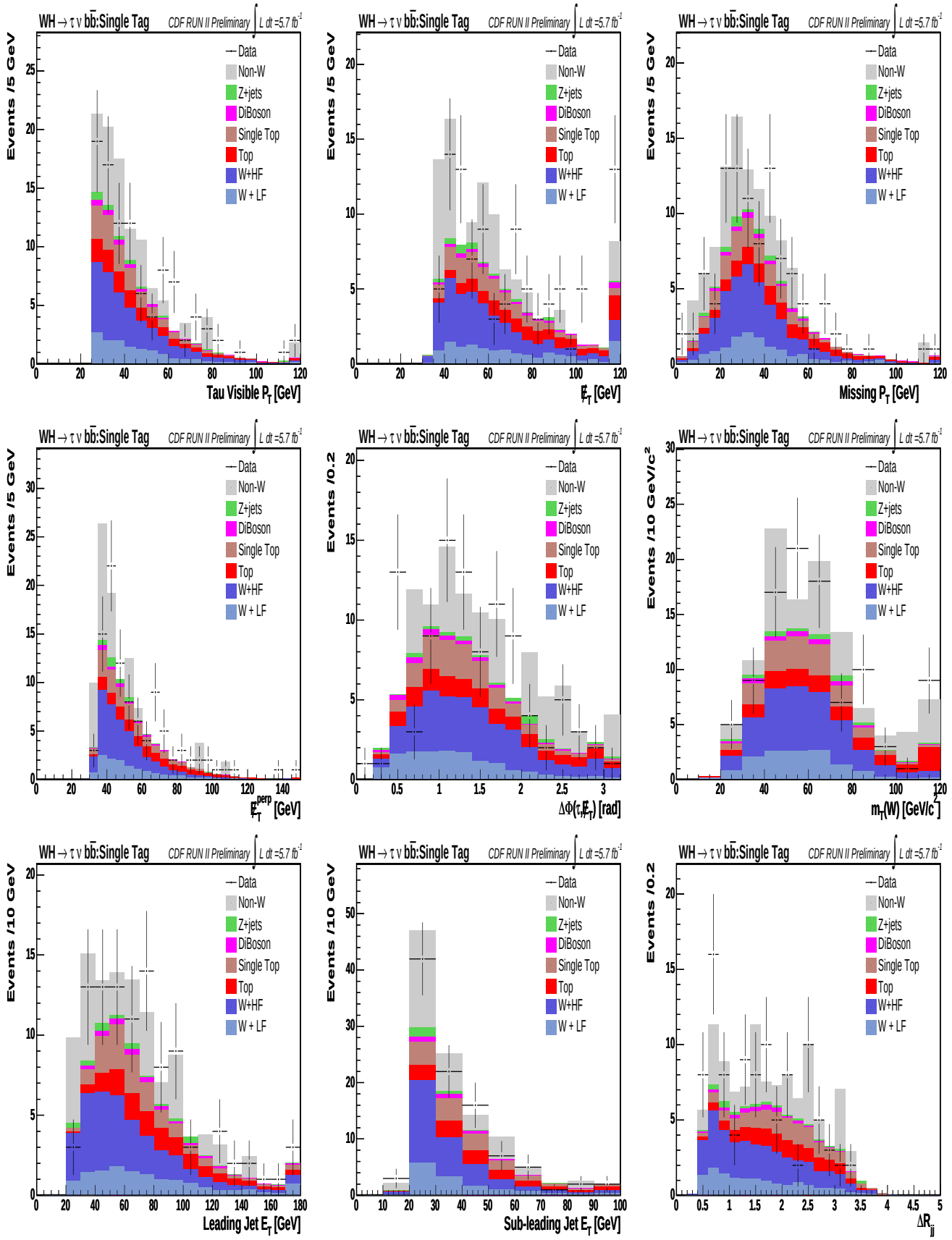

FIG. 4: Comparison between expected and observed distributions in different kinematic variables, for the sample with one b-tagged jet and $\not\!\!E_{\rm T}^{perp} > 34$GeV. The background predictions are able to describe the data within statistical uncertainty.

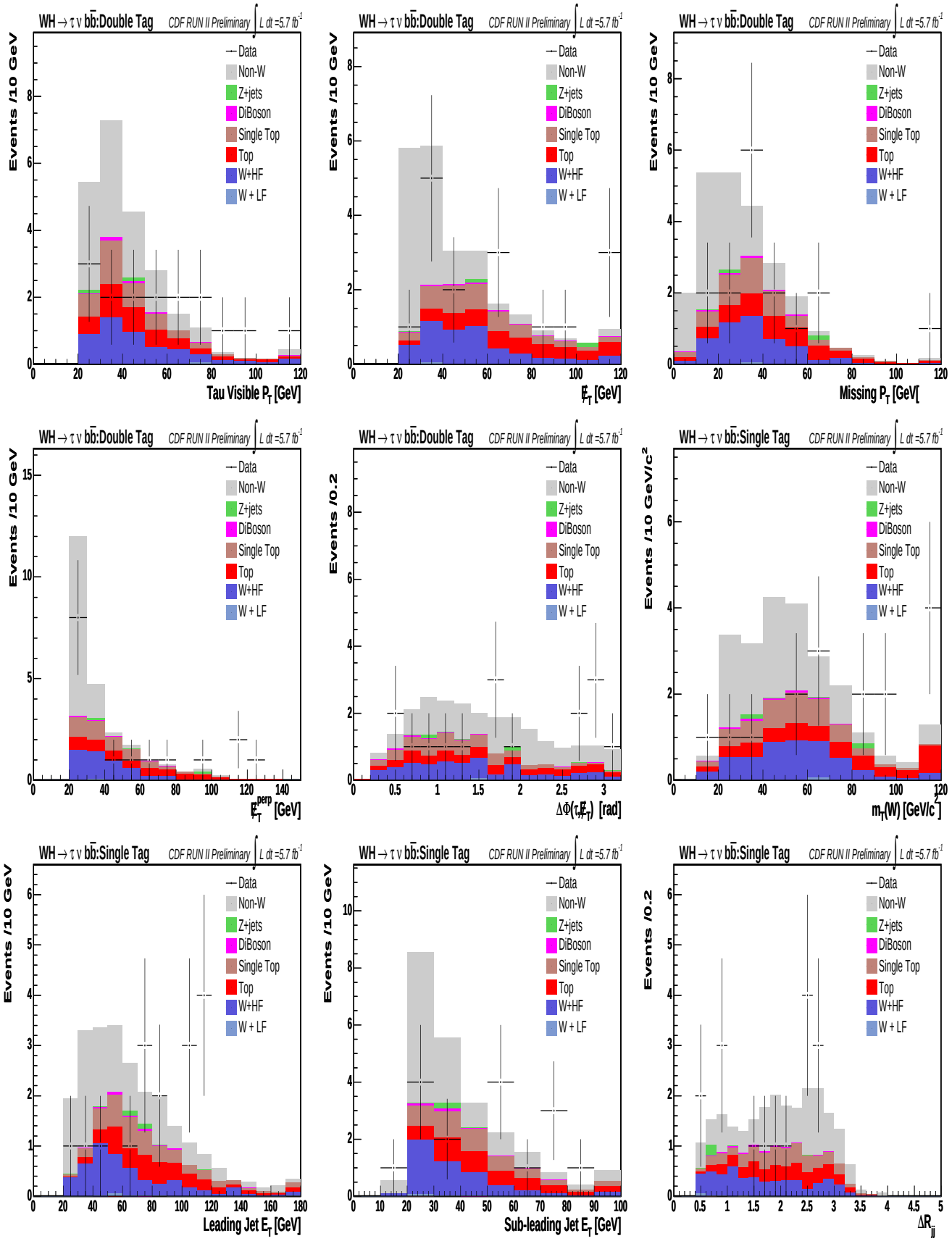

FIG. 5: Comparison between expected and observed distributions in different kinematic variables, for the sample with two b-tagged jets and $\not\!\!E_{\rm T}^{perp} > 20$GeV. The background predictions are able to describe the data within statistical uncertainty.

CDF Run II Preliminary, $WH \to \tau\nu b\bar{b}$, $5.7 fb^{-1}$
Single Tagged Sample, $\not\!\!E_{\rm T}^{perp} > 34$ GeV

NJets	1jet	2jets	3jets	4jets
WW	1.01 ± 0.20	1.96 ± 0.37	0.64 ± 0.13	0.14 ± 0.03
WZ	0.37 ± 0.07	0.69 ± 0.13	0.18 ± 0.04	0.02 ± 0.01
ZZ	0.04 ± 0.01	0.04 ± 0.01	0.01 ± 0.00	0.01 ± 0.00
Single top (t-chan)	2.75 ± 0.52	6.71 ± 1.26	1.84 ± 0.35	0.35 ± 0.07
Single top (s-chan)	6.05 ± 1.20	7.93 ± 1.57	2.15 ± 0.43	0.43 ± 0.09
$Z \to ee$	0.10 ± 0.06	0.00 ± 0.00	0.00 ± 0.00	0.00 ± 0.00
$Z \to \tau\tau$	5.92 ± 1.17	2.64 ± 0.53	0.57 ± 0.13	0.01 ± 0.01
$t\bar{t}$	2.29 ± 0.43	12.70 ± 2.35	20.06 ± 3.71	14.67 ± 2.72
Mistag	38.34 ± 1.41	13.67 ± 0.91	3.08 ± 0.54	0.67 ± 0.45
$Wb\bar{b}$	17.81 ± 5.37	17.07 ± 5.17	3.95 ± 1.28	0.94 ± 0.51
$Wc\bar{c}$	8.53 ± 2.60	8.24 ± 2.52	2.48 ± 0.81	0.56 ± 0.31
Wc	10.37 ± 3.16	4.32 ± 1.32	0.38 ± 0.12	0.02 ± 0.01
Non-W	50.68 ± 8.11	34.55 ± 6.77	12.70 ± 4.01	5.66 ± 2.83
Total Background	144.27 ± 10.81	110.51 ± 9.57	48.04 ± 5.73	23.48 ± 3.99
WH ($m_H = 115$ GeV/c^2)	0.11 ± 0.02	0.30 ± 0.05	0.08 ± 0.01	0.01 ± 0.00
Observed	155.00	100.00	41.00	18.00

TABLE I: Expected and observed number of events with $\not\!\!E_{\rm T}^{perp} > 34$ GeV, in the Single Tag sample (column corresponding to 2 jets) and for events with different number of jets.

CDF Run II Preliminary, $WH \to \tau\nu b\bar{b}$, $5.7 fb^{-1}$
Double Tagged Sample, $\not\!\!E_{\rm T}^{perp} > 20$ GeV

NJets	2jets	3jets	4jets
WW	0.03 ± 0.02	0.04 ± 0.02	0.04 ± 0.02
WZ	0.21 ± 0.05	0.04 ± 0.01	0.02 ± 0.01
ZZ	0.01 ± 0.00	0.00 ± 0.00	0.00 ± 0.00
Single top (t-chan)	2.84 ± 0.54	1.00 ± 0.19	0.18 ± 0.04
Single top (s-chan)	0.88 ± 0.18	0.76 ± 0.15	0.18 ± 0.04
$Z \to ee$	0.00 ± 0.02	0.00 ± 0.00	0.00 ± 0.00
$Z\tau\tau$	0.24 ± 0.14	0.23 ± 0.09	0.00 ± 0.00
$t\bar{t}$	3.57 ± 0.67	8.45 ± 1.57	9.07 ± 1.68
Mistag	0.11 ± 0.01	0.05 ± 0.01	0.02 ± 0.01
$Wb\bar{b}$	4.42 ± 1.36	1.25 ± 0.41	0.27 ± 0.17
$Wc\bar{c}$	0.24 ± 0.07	0.10 ± 0.03	0.03 ± 0.02
Wc	0.20 ± 0.06	0.02 ± 0.01	0.00 ± 0.00
Non-W	11.11 ± 1.21	4.21 ± 0.68	1.52 ± 0.50
Total Background	23.88 ± 2.03	16.14 ± 1.78	11.33 ± 1.76
WH ($m_H = 115$ GeV/c^2)	0.14 ± 0.03	0.04 ± 0.01	0.01 ± 0.00
Observed	16.00 ± 0	17.00 ± 0	11.00 ± 0

TABLE II: Expected and observed number of events with $\not\!\!E_{\rm T}^{perp} > 20$ GeV, in the Double Tag sample (column corresponding to 2 jets) and for events with different number of jets.

efficiency is dominated by the uncertainty on the data/MC scale factors. Other uncertainties on the initial- final-state radiation and the parton distribution functions contribute to a smaller extent to the overall uncertainty. The effect of the jet energy scale uncertainty (JES) is evaluated by varying the jet energy correction by $\pm 1\sigma$, where σ represent its uncertainty. The uncertainty in the shape of the di-jet invariant mass due to the JES is also taken into account. A summary of the systematic uncertainties on the signal acceptance and background prediction is given in Tables III for the Single tag sample, and IV for the Double tags sample.

CDF Run II Preliminary, $WH \to \tau\nu b\bar{b}$, Single Tag Sample, $5.7 fb^{-1}$

Systematic Uncertainty (%)	Signal	Non-W	W+HF	W+LF	Z+jets	DiBoson	$t\bar{t}$ and Single t
b-tagging	4.3	-	4.3	-	4.3	4.3	4.3
Tau Trigger and ID	17.	-	17.	17.	17.	17.	17.
JES	2. - shape						
Heavy Flavor Fraction			30.				
Mistag Probability				7.			
Non-W normalization		20.					
ISR-FSR-PDF	2.						

TABLE III: List of Systematic uncertainties affecting the signal and backgrounds in the Single Tag sample.

CDF Run II Preliminary, $WH \to \tau\nu b\bar{b}$, Double Tag Sample, $5.7 fb^{-1}$

Systematic Uncertainty (%)	Signal	Non-W	W+HF	W+LF	Z+jets	DiBoson	$t\bar{t}$ and Single t
b-tagging	8.6	-	8.6	-	8.6	8.6	8.6
Tau Trigger and ID	17.	-	17.	17.	17.	17.	17.
JES	2. - shape						
Heavy Flavor Fraction			30.				
Mistag Probability				10.			
Non-W normalization		11.					
ISR-FSR-PDF	2.						

TABLE IV: List of Systematic uncertainties affecting the signal and backgrounds in the Double Tag sample.

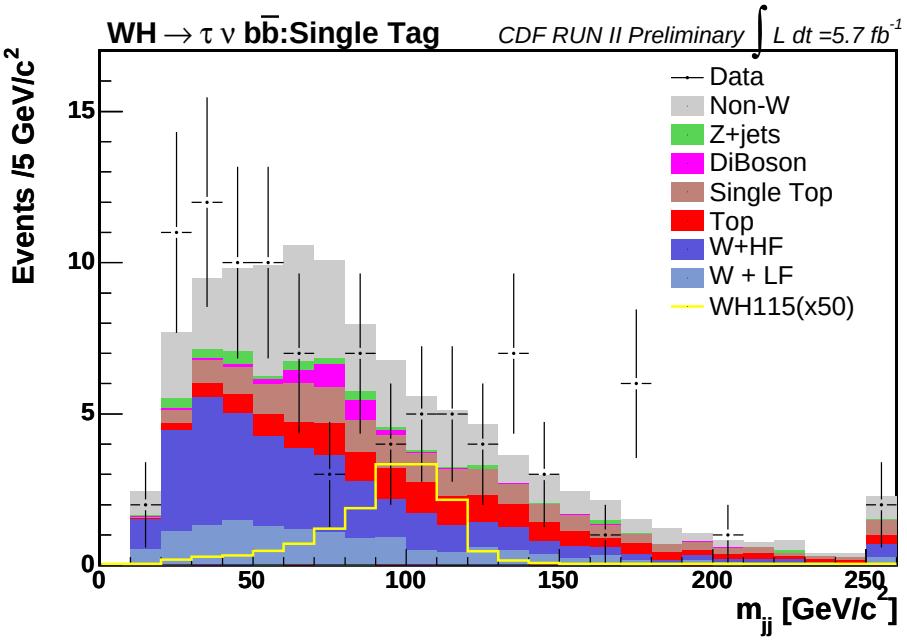

FIG. 6: Di-jet invanrian mass distribution, for events with one b-tagged jet. The background templates are normalized to the expected yields listed in table I. The yellow curve correspond to the Higgs boson signal contribution ($m_H = 115 GeV/c^2$), if the production cross section was 50 time the one predicted by the Standard Model.

VII. RESULTS

To optimize the sensitivity, we perform a direct search for an excess in the di-jet invariant mass spectrum for the single and double b-tagged W+2 jet events separately. Fig. 6 and Fig. 7 show the di-jet mass distributions for each b-tagging category. The data and predictions are in agreement within the uncertainties, and no evidence of a signal is present. A binned likelihood fit of the di-jet invariant mass distribution is performed to test for a potential Higgs boson signal. In the absence of an observed excess, we set upper limits on $\sigma(p\bar{p} \to H) \times BR(H \to b\bar{b}$ normalized to the SM prediction, as a function the Higgs boson mass. The single and double b-tagged samples have similar sensitivity. The expected and observed 95% C.L. limit for the combined sample (Single Tag and Double Tag samples) are shown in table V and in figure 8.

VIII. CONCLUSIONS

We presented the results of a search for the standard model Higgs boson decaying to $b\bar{b}$, produced in association with a W boson in the $WH \to \tau\nu b\bar{b}$ final state. We find that for the dataset corresponding to an integrated luminosity of 5.7 fb^{-1}, the data agree with the SM expectations within the uncertainties. We therefore set upper limits on $\sigma(p\bar{p} \to W^{\pm}H) \times \mathrm{Br}(H \to b\bar{b})$. We find that the observed (expected) upper limits range from 13.4 (30.0) $\times$ SM to 488.0 (395.3) $\times$ SM for the Higgs boson masses ranging from 100 GeV/c^2 through 150 GeV/c^2. For a mass of of 115

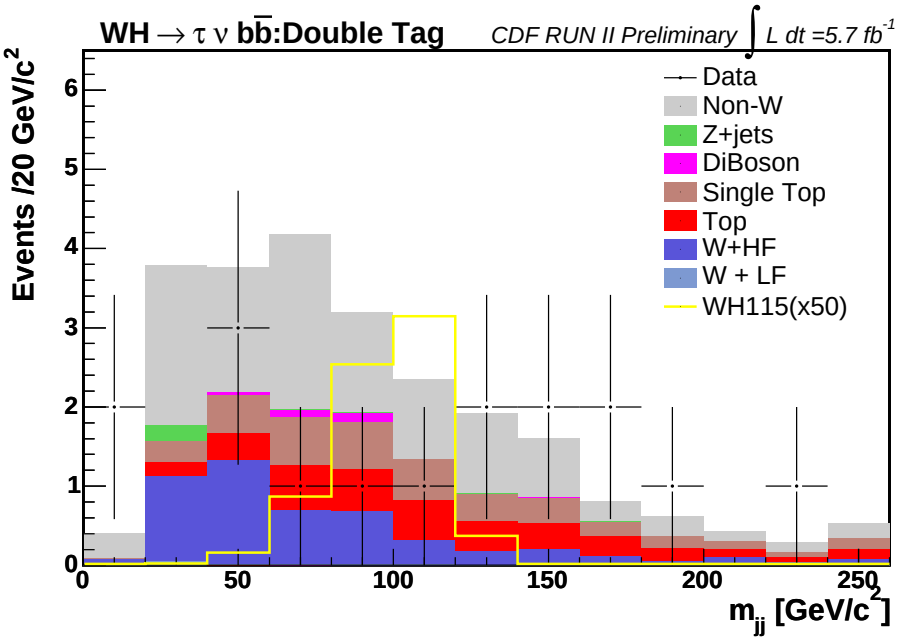

FIG. 7: Di-jet invariant mass distribution, for events with two b-tagged jet. The background templates are normalized to the expected yields listed in table II. The yellow curve correspond to the Higgs boson signal contribution ($m_H = 115 GeV/c^2$), if the production cross section was 50 time the one predicted by the Standard Model.

CDF Run II Preliminary, $WH \to \tau\nu b\bar{b}$, $5.7 fb^{-1}$
$\sigma(95\text{ C.L. limit})/\sigma_{S.M.} * BR(H \to b\bar{b})$

m_H	Observed	-2σ	-1σ	Median	$+1\sigma$	$+2\sigma$
100	13.4	12.9	20.4	30.0	43.3	60.4
105	16.7	15.2	23.8	35.2	50.4	70.0
110	24.0	17.1	26.9	40.1	57.4	82.1
115	28.7	19.7	31.7	46.6	67.0	94.0
120	33.9	24.7	38.6	57.1	82.0	115.1
125	53.4	29.7	46.5	68.9	98.6	136.7
130	82.6	37.7	59.7	87.7	126.3	175.0
135	112.7	50.3	79.8	118.1	168.3	234.7
140	186.5	76.3	118.1	174.7	248.4	345.3
145	294.6	107.0	169.8	248.7	355.8	505.2
150	488.0	172.8	265.7	395.3	569.8	787.6

TABLE V: Observed and expected limits on the ratio of the measured cross section to the one predicted by the Standard Model, for the Single and Double Tag samples combined.

GeV/c^2 the upper limit is 28.7 (46.6) × SM.

Acknowledgments

We thank the Fermilab staff and the technical staffs of the participating institutions for their vital contributions. This work was supported by the U.S. Department of Energy and National Science Foundation; the Italian Istituto Nazionale di Fisica Nucleare; the Ministry of Education, Culture, Sports, Science and Technology of Japan; the Natural Sciences and Engineering Research Council of Canada; the National Science Council of the Republic of China; the Swiss National Science Foundation; the A.P. Sloan Foundation; the Bundesministerium für Bildung und Forschung, Germany; the Korean World Class University Program, the National Research Foundation of Korea; the

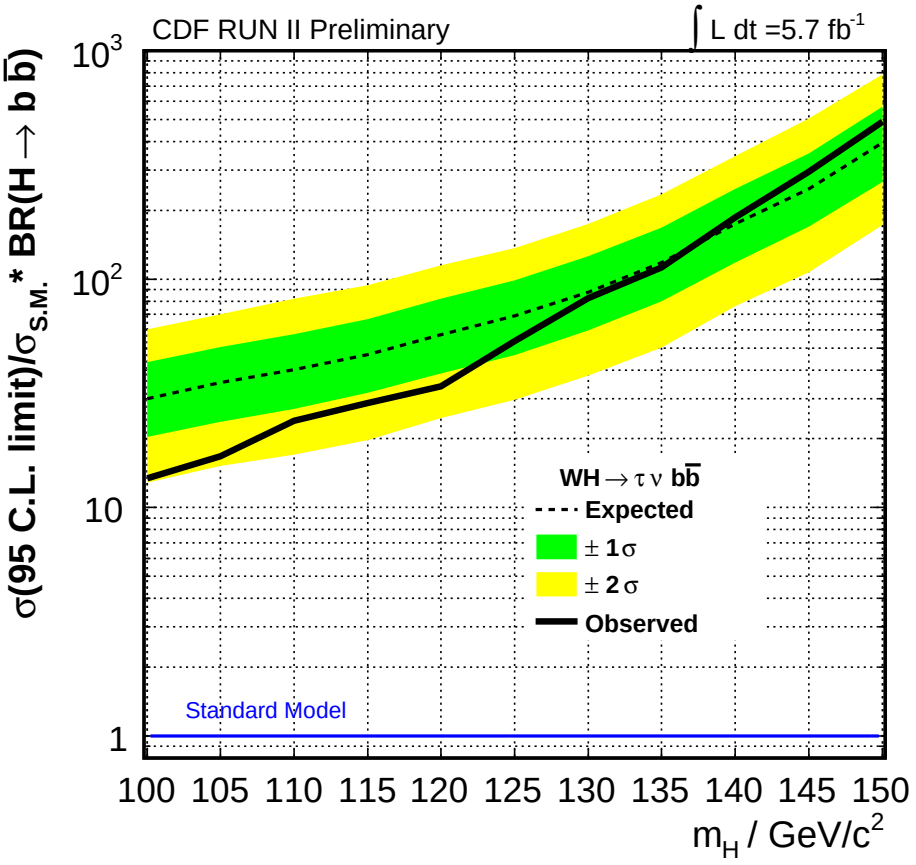

FIG. 8: Expected and observed 95% C.L. limits, for the combined limit of the Single and Double Tagged samples.

Science and Technology Facilities Council and the Royal Society, UK; the Institut National de Physique Nucleaire et Physique des Particules/CNRS; the Russian Foundation for Basic Research; the Ministerio de Ciencia e Innovación, and Programa Consolider-Ingenio 2010, Spain; the Slovak R&D Agency; the Academy of Finland; and the Australian Research Council (ARC).

[1] The CDF, D0 Collaborations, the Tevatron New Phenomena, Higgs Working Group arXiv:1107.5518v1 [hep-ex]
[2] LEP Electroweak Working Group, `http://lepewwg.web.cern.ch/LEPEWWG/`
[3] ALEPH, DELPHI, L3, OPAL. The LEP Working Group for Higgs Boson Searches, Phys. Lett **B565** 61 (2003).
[4] T.Aaltonen *et al.* (CDF Collaboration), CDF Public Note 10596 (2011).
[5] F. Abe *et al.*, Nucl. Instrum. Methods Phys. Res. A **271**, 387 (1988);
D. Amidei *et al.*, Nucl. Instum. Methods Phys. Res. A **350**, 73 (1994);
F. Abe *et al.*, Phys. Rev. D **52**, 4784 (1995);
P. Azzi *et al.*, Nucl. Instrum. Methods Phys. Res. A **360**, 137 (1995);
The CDF II Detector Technical Design Report, Fermilab-Pub-96/390-E.
[6] P. T. Lukens (CDF IIb) (2003), FERMILAB-TM-2198
[7] B. Bhatti *et al.*, Nucl. Instum. Methods **A556**, 375 (2006);

[8] A. Abulencia *et al.*, Phys. Rev. **D71**, 072005 (2005).

[9] P. Edén, C. Friberg, L. Lönnblad, G. Miu, S. Mrenna, E. Norrbin, and T. Sjöstrand, Computer Phys. Commun. **135** (2001) 238.
[10] M.L. Mangano *et al.*, JHEP 0307:001, 2003.